Computers and Mathematics with Applications 67 (2014) 34–51

Contents lists available at ScienceDirect

Computers and Mathematics with Applications

journal homepage: www.elsevier.com/locate/camwa

A novel model for biofilm growth and its resolution by using the hybrid immersed interface-level set method

Patricio Cumsille [a,b,*], Juan A. Asenjo [c], Carlos Conca [d,b]

[a] Grupo de Matemáticas Aplicadas, Departamento de Ciencias Básicas, Facultad de Ciencias, Universidad del Bío-Bío, Campus Fernando May, Av. Andrés Bello s/n, Casilla 447, Chillán, Chile

[b] Institute for Cell Dynamics and Biotechnology: a Centre for Systems Biology, University of Chile, Beauchef 850, Santiago, Chile

[c] Centre for Biochemical Engineering and Biotechnology and Institute for Cell Dynamics and Biotechnology: a Centre for Systems Biology, University of Chile, Beauchef 850, Santiago, Chile

[d] Departamento de Ingeniería Matemática (DIM) and Centro de Modelamiento Matemático (CMM), Universidad de Chile (UMI CNRS 2807), Av. Blanco Encalada 2120, Casilla 170-3, Correo 3, Santiago, Chile

ARTICLE INFO

Article history:
Received 21 March 2013
Received in revised form 7 September 2013
Accepted 22 October 2013

Keywords:
Biofilm modeling
Hele-Shaw flow
Immersed interface method
Level set method

ABSTRACT

In this work we propose a new model to simulate biofilm structures ("finger-like", as well as, compact structures) as a result of microbial growth in different environmental conditions. At the same time, the numerical method that we use in order to carry out the computational simulations is new to the biological community, as far as we know. The use of our model sheds light on the biological process of biofilm formation since it simulates some central issues of biofilm growth: the *pattern formation of heterogeneous structures, such as finger-like structures*, in a substrate-transport-limited regime, and the formation of more compact structures, in a growth-limited-regime. The main advantage of our approach is that we consider several of the most relevant aspects of biofilm modeling, particularly, the existence and evolution of a biofilm–liquid interface. At the same time, in order to perform numerical simulations, we have used sophisticated numerical techniques based on mixing the immersed interface method and the level-set method, which are well described in the present work.

1. Introduction

Biofilm processes are of interest to researchers in a wide variety of fields including purposes of filtration, bioremediation, or barrier formation. A biofilm is a complex and heterogeneous matrix of microorganisms attached to and growing on a surface. Biofilms are most often found on solid substrates that are exposed to an aqueous solution [1]. The liquid usually supplies nutrients (substrates) utilized by the microorganisms in the biofilm, while pieces of biofilm solids detach from the biofilm compartment and move to the bulk-liquid compartment. The exchange between the biofilm and the liquid may lead to spatially heterogeneous architectures that can induce complex flow patterns and affect mass transport. Thus, mass transport due to diffusion and advection in the fluid compartment should be explicitly considered. The latter implies that the hydrodynamic flow field should be taken into account as well [2–6]. The accumulation of biofilm depends on hydrodynamic processes that bring cells to the biofilm surface, physical–chemical properties that determine the propensity of microbes to attach to the biofilm, and environmental characteristics such as substrate concentrations that determine biofilm growth. Cells may also be removed from the biofilm by biological processes or flow properties that lead to desorption and detachment [1].

* Corresponding author at: Grupo de Matemáticas Aplicadas, Departamento de Ciencias Básicas, Facultad de Ciencias, Universidad del Bío-Bío, Campus Fernando May, Av. Andrés Bello s/n, Casilla 447, Chillán, Chile.
E-mail addresses: pcumsill@gmail.com, pcumsille@ubiobio.cl (P. Cumsille), juasenjo@ing.uchile.cl (J.A. Asenjo), cconca@dim.uchile.cl (C. Conca).

0898-1221/$ – see front matter
http://dx.doi.org/10.1016/j.camwa.2013.10.008

In this paper, we study a model that considers most of the key aspects mentioned in the previous paragraph. The only feature that we do not consider is the attachment/detachment of cells to the biofilm. Instead, we consider a biofilm already attached to a surface and study the effects of the substrate, the pressure inside of the biofilm, as well as the hydrodynamic flow field in its growth. A model, which considers attachment/detachment, would require discrete representations of microorganisms that may hold them together or, if fluid stress is large, the fluid may yield and release microbes [1]. There is consensus that the most relevant aspects in a biofilm model are, on the one hand, the existence of an interface between the biofilm and the liquid and, on the other hand, the biofilm structure, which is affected by the influence of biomass growth in relation to substrate transport. Porous biofilms, with many channels and voids between the "finger-like" or "mushroom" outgrowth, were obtained in a substrate-transport-limited regime. Conversely, compact and smooth biofilms occurred in systems limited by the biomass growth rate and not by the substrate transfer rate [3].

In this paper we propose a new model for biofilm formation and use the *immersed interface method* (IIM), coupled to the *level set method* for its numerical implementation. The IIM, first introduced by LeVeque and Li [7] to model elliptic problems with discontinuous coefficients and singular source terms, has evolved (coupled with others methods) into a general blended method that can be used to study two-phase flows, among others applications. The name of the method derives from the fact that the interface between both fluids is modeled as a free boundary, which may have a complex structure, immersed in a *unique* fluid. Thus, this interface defines and separates different regions inside the fluid.

Biofilm research is an active area within the microbiology community, as researchers recognize that attached organisms often predominate in a wide range of medical, natural, and industrial environments. Consequently, effective biofilm models could be a fast and cost-effective aid for biologists. The problem of biofilm growth has been studied intensively in the recent years. Here we mention the following papers, which are closely related with the use of partial differential equations based models:

- The paper by Dockery and Klapper [8], in which a biofilm model is considered to be analogous to a fluid flowing in a porous medium. These authors compute the velocity and pressure of the biofilm, modeling it as an incompressible viscous fluid.
- The paper by Eberl and Demaret [9] studies a biofilm model based on a degenerated diffusion–reaction equation, in which the biomass density of the biofilm is the unknown, and assuming a non-linear dependence of the diffusion coefficient on this biomass density.
- The paper by Dillon et al. [1], in which a biofilm model is studied using a variant of the *immersed boundary method*, introduced by Peskin [10] in the modeling of blood flow in the heart. This model incorporates various hydrodynamic coupled effects like reaction, diffusion and convection of a substrate, as well as the chemotactic response of microbes to attachment/detachment (both cell–cell aggregation and cell-wall adhesion). The problem of this model is the fact that it is too difficult to be implemented and requires numerical resolution of Navier–Stokes equations with a singular force term.
- Studies by others authors [3–6] analyze a biofilm model based on a hybrid differential-discrete cellular automaton approach. Picioreanu et al. [3] characterized the complete biofilm structure (surface and volume structure) and found that a key factor affecting biofilm structure is the influence of biomass growth in relation to the substrate transfer. These authors represent soluble components (e.g., substrates) in a continuous field, whereas a discrete mapping is used for the solid components (e.g., biomass). They validate their results with measured data from a well-characterized system: the growth of immobilized cells in a gel matrix. Finally, Picioreanu et al. [6] investigated the effect of convective and diffusive substrate transport on biofilm heterogeneity. They obtained similar results as in their previous work, namely that variations in external mass transfer resistance (due to convection and flow-driving mechanisms) have less effects on biofilm development. Thus, they concluded that the determining factor is still the internal resistance to substrate transport.
- The paper by Alpkvist and Klapper [11] proposes a model for the heterogeneous growth of biofilm systems with multiple species and multiple substrates. This paper is a generalization of the previous 2-D model [8] and of the earlier 1-D model [12], and enabled the authors to perform simulations that may represent biofilm systems for which a one-dimensional model is an inadequate description or, conversely, may under some circumstances, verify adequacy of one dimensional representation.
- The paper by Duddu et al. [13] proposes a hybrid extended Finite Element Method (XFEM)—level set method for the growth of biofilms. This method does not require an explicit representation of the biofilm–fluid interface (as in our method). These authors obtained finger formation and incipient tip splitting, behaviors observed in real biofilms.
- The paper by Cogan [14] proposes a model of biofilm disinfection in two dimensions, where the biofilm is treated as a viscous fluid immersed in a fluid of less viscosity. The motion of the fluid is coupled to the biofilm inducing motion in it. Both the biofilm and the bulk fluid are dominated by viscous forces; hence the Reynolds number is negligible and the appropriate equations are Stokes equations. In our paper, we also model the biofilm as a slow viscous fluid, but we assume that the biofilm as well as the liquid satisfies the Hele-Shaw equations instead of the Stokes equations.
- The paper by Ward et al. [15] proposes mathematical models for the formation, growth and quorum sensing activity of bacterial biofilms in its early development.
- Similarly in others papers [16–18] a hierarchy of mathematical models for antibacterial therapies targeted at the primary quorum-sensing system of a well-mixed, planktonic population and an early-stage (closely packed) biofilm is developed.
- The papers by Zhang et al. [19,20] develop a hierarchy of phase field-based models for biofilms in 1-D and 2-D respectively. In [19] a set of phase field models for biofilms using the one-fluid two-component formulation is derived, in which the combination of extracellular polymeric substances (EPS, or polymer networks) and the bacteria is effectively modeled as one fluid component, while the collective ensemble of nutrient substrates and the solvent are modeled as the

other. Then, in [20] the biofilm–flow interaction is studied resulting in biofilm growth, deformation and detachment phenomena in a cavity and shear flow using the phase field model developed before.

Despite several studies about of biofilm growth, we have developed a totally novel model that could contribute to the understanding of this very interesting problem. Our model has been specially designed to capture real characteristics of a biofilm, namely, as it has been empirically observed, that many biofilms grow to form finger-like structures. In order to capture this phenomenon in a suitable way, we have developed a totally novel model that mirrors the growth of a biofilm to a Hele-Shaw flow. We do this since the Hele-Shaw flow can reproduce this type of growth quite accurately in the case of two fluids with different viscosities separated by an interface. On the other hand, the IIM has been coupled with the level-set method in several papers including the Hele-Shaw flow to compute unstable fronts in different contexts [21–24] but it has never been used in the past to solve biofilm models. In the present work, we have applied this approach for simulating the evolution of a biofilm, and as far as we know it is the first time this is applied to the field of biology. This is a central point of this paper. The IIM has been implemented since it offers an efficient approach to model interface problems [7,21,25], and in coupling this with the Level-Set method as it was originally designed to deal with moving free-boundary problems [26,27].

2. The mathematical model

Since a biofilm behaves as a very viscous fluid with large viscosity relative to water [11], it is valid to think that biofilm dynamics would behave as a slow viscous fluid. Thus, we assume that the system composed of a biofilm and a liquid that supplies it nutrients (substrates), behaves as a Hele-Shaw flow, that is, two fluids with different viscosities, separated by an interface, that flow with relatively low velocity, from the regions with high pressure towards those with low pressure (opposite the direction of increasing gradient). A Hele-Shaw type-like modeling was chosen primarily because it is well known among physicists that is able to reproduce finger-shaped structures, which is a prominent feature in biofilm formation.

Let $\Omega := (0, L_X) \times (0, L_Z) \subset \mathbb{R}^2$ be a region of the plane, in which we distinguish two subregions: the region $\Omega_1(t)$ which represents the liquid, and the region $\Omega_2(t)$ which represents the biofilm, separated by an interface $\Gamma(t)$. We remark that such an interface is an element of the mathematical modeling and does not correspond to an observed feature in real biofilms. However, most of biofilm models (in particular all biofilm models discussed in this paper) include such a hypothetical interface as well, either explicitly by construction or implicitly as a consequence of the model equations.

As said before, the whole medium (biofilm plus liquid) is modeled as a slow two-phase flow, whose phases are fluids with different viscosities. In accordance with the Hele-Shaw flow, we have

$$\mathbf{u} = -\lambda \nabla p \quad \text{in } \Omega,$$

where $\mathbf{u}$ is the velocity vector field ($\mathrm{m\,s^{-1}}$), p is the pressure field ($\mathrm{kg\,m^{-1}\,s^{-2}}$) and λ ($\mathrm{kg\,m^3\,s}$) is a parameter which varies in form inversely proportional to the viscosities (see p. 271 in [25]). Although, by simplicity we have assumed in our simulations that λ is a small constant, in order to take into account the fact that the biofilm behaves as a fluid with large viscosity.

For modeling the fact that the biofilm may be growing (or decaying) at any given location, we impose that the biofilm contains sources and/or sinks [8]. This is, the velocity field in the biofilm compartment is not divergence-free, i.e.,

$$\nabla \cdot \mathbf{u} = g,$$

where g is a prescribed source (or sink) term ($\mathrm{s^{-1}}$). This yields the following relation:

$$-\lambda \nabla^2 p = g, \tag{1}$$

which holds in the biofilm compartment. The normal velocity of the biofilm interface Γ is $\lambda \nabla p \cdot n|_{\Gamma^-}$, where n is the unitary upward normal and Γ^- indicates the evaluation of $\nabla p \cdot n$ from the side of the biofilm region. Due to the fact that the liquid does not grow or decay (indeed water is an incompressible fluid), it is quite natural to impose that the velocity field in the liquid compartment is divergence-free, i.e.,

$$\nabla \cdot \mathbf{u} = 0,$$

and therefore

$$-\lambda \nabla^2 p = 0, \tag{2}$$

in the liquid compartment.

In order to uniquely determine the pressure from Eqs. (1) and (2), we have to add external boundary conditions. For instance, we assume that no biofilm goes in or out by the bottom of Ω:

$$\lambda \left.\frac{\partial p}{\partial z}\right|_{z=0} = 0.$$

Moreover, for numerical convenience, we assume that p is periodic in the x-direction. On the other hand, assuming that on the top of the domain there is a constant pressure (atmospheric pressure), and since this is always defined up to an additive constant, without loss of generality, we will impose the following boundary condition:

$$p = 0 \quad \text{on } z = L_Z.$$

In the Hele-Shaw flow, g represents the injection of a low-viscosity fluid into a high-viscosity one. The evolution of such a system exhibits the development of finger-like structures, which is precisely a feature observed in real behavior of biofilm formation. In our biofilm model g represents the local biomass volumetric flow rate (s^{-1}), i.e., the biomass volumetric flow rate through a closed surface Σ can be calculated as the integral of g over the volume enclosed by Σ. The function g is determined by local conditions in the biofilm and also, in principle, by the biofilm history. For simplicity purposes, however, we assume that g depends only on the concentration $S(x, z, t)$ of a single limiting substrate, e.g., oxygen or glucose (kg m^{-3}). In particular, we assume that $g = g(U(S))$, where $U(S)$ is the so-called *usage function* or *substrate uptake rate*, which indicates the reaction rate of substrate usage (kg m^{-3} s^{-1}). Note that U and g do not explicitly depend on time or space in the model presented here. Our choice consists of the following Monod-type reaction kinetics [6]:

$$U(S) = \delta_U U_{Sm}(1+\mu)\frac{S}{K_S + S}. \tag{3}$$

The parameters U_{Sm} and K_S represent the maximum substrate consumption rate (kg m^{-3} s^{-1}) and the saturation constant for substrate (kg m^{-3}), respectively. Moreover δ_U and μ are dimensionless quantities representing a scaling parameter (introduced for computational convenience) and a maintenance coefficient, respectively.

A relation similar to $U(S)$ is also often used for the local biomass volumetric flow rate g. In the present model, we define g by the relation:

$$g(U) = \delta_g \mu_m \left[(1+\mu)\frac{S}{K_S + S} - \mu \right]. \tag{4}$$

The parameter μ_m is the maximum biomass growth rate (s^{-1}), whereas δ_g is a dimensionless quantity representing a scaling parameter (introduced for computational convenience).

The presence of microorganisms at the biofilm/liquid interface influences both the flow dynamics and the substrate field [1]. The equations which describe the advection, diffusion, and consumption of a single chemical species within the biofilm-filled pores are

$$S_t + \nabla \cdot (S\mathbf{u}) - D_S \nabla^2 S = 0, \quad \text{in } \Omega_1(t),$$
$$S_t + \nabla \cdot (S\mathbf{u}) - D_S \nabla^2 S = -U(S), \quad \text{in } \Omega_2(t),$$

coupled with the following boundary conditions: $S|_{z=L_Z} = S_m$ (the substrate concentration is at its maximum level at the top of Ω) and $\frac{\partial S}{\partial z}\big|_{z=0} = 0$ (no substrate goes in or out by the bottom of Ω). Moreover, for numerical convenience, we assume that S is periodic in the x-direction. In equations above D_S stands for the diffusion coefficient of the substrate (m^2 s^{-1}).

Due to the presence of the interface, it is necessary to impose internal boundary conditions or transmission conditions on the interface. These conditions must be physically reasonable and represent the dynamical growth of the biofilm front, as it was previously specified (that is, biofilm grows to form eventually finger-like structures). These conditions are given by the Hele-Shaw flow. They can be expressed as follows:

$$[p] = \gamma\kappa \quad \text{on } \Gamma(t), \tag{5}$$
$$[\lambda p_n] = 0 \quad \text{on } \Gamma(t), \tag{6}$$

where $[f]$ denotes the jump of a function f across the interface $\Gamma(t)$, i.e., the difference of the limiting values of f from each side of the interface; $\gamma > 0$ is the surface tension coefficient (kg s^{-2}) and $\kappa = \kappa(x, z, t)$ is the mean curvature at the point (x, z) on the interface $\Gamma(t)$ (m^{-1}).

Condition (5) allows the substrate to penetrate into the biofilm, in such a way that the biofilm/liquid interface could exhibit a fingering phenomenon. As in a Hele-Shaw flow, this is thanks to the surface tension which behaves in such a way that the smaller the surface tension is, the more unstable is the biofilm–flow [21]. Hence, this model also provides insight in the physical–biological process of biofilm formation in the sense that it reproduces, on one hand, the interface between the biofilm and the surrounding medium and, on the other hand, eventually the pattern formation of finger-like structures, which can be observed in real biofilm growth.

Finally, for the substrate, we assume natural transmission conditions, i.e.,

$$[S] = 0 \quad \text{on } \Gamma(t),$$
$$\left.\frac{\partial S}{\partial n}\right|_{\Gamma^+} = \left.\frac{\partial S}{\partial n}\right|_{\Gamma^-} \quad \text{on } \Gamma(t).$$

3. Dimensionless form and parameters of the model

Gathering the equations of the previous section, we have the following model:

$$-\lambda\nabla^2 p = g(U)\chi_{\Omega_2(t)} \quad \text{in } \Omega, \tag{7}$$

$$
\begin{aligned}
&[p] = \gamma\kappa \quad \text{on } \Gamma(t),\\
&[\lambda p_n] = 0 \quad \text{on } \Gamma(t),\\
&p = 0 \quad \text{on } z = L_Z,\\
&\lambda p_z = 0 \quad \text{on } z = 0,\\
&p(0,z) = p(L_X,z) \quad \forall z \in (0,L_Z),\\
&S_t + \nabla\cdot(S\mathbf{u}) - D_S\nabla^2 S = -U(S)\chi_{\Omega_2(t)} \quad \text{in } \Omega,\\
&[S] = 0 \quad \text{on } \Gamma,\\
&[S_n] = 0 \quad \text{on } \Gamma,\\
&S = S_m \quad \text{on } z = L_Z,\\
&S_z = 0 \quad \text{on } z = 0,\\
&S(0,z) = S(L_X,z) \quad \forall z \in (0,L_Z).
\end{aligned}
\tag{8}
$$

In Eqs. (7) and (8) we have denoted by $\chi_{\Omega_2(t)}$ the characteristic function of the biofilm compartment at time t.

For numerical reasons, it is better to use a dimensionless model. Setting the dimensionless variables:

$$
\begin{aligned}
&\bar{x} = \frac{x}{L_Z}; \qquad \bar{z} = \frac{z}{L_Z}; \qquad \bar{L}_X = \frac{L_X}{L_Z}; \qquad \bar{L}_Z = \frac{L_Z}{L_Z} = 1;\\
&\bar{t} = \frac{t}{T}; \qquad \bar{S} = \frac{S}{S_m}; \qquad \bar{p} = \frac{\lambda\nu}{D_S G}p;\\
&\bar{\mathbf{u}} = -\nabla_{(\bar{x},\bar{z})}\bar{p}; \qquad \bar{g} = \frac{\nu S_m}{U_{Sm}}g; \qquad \bar{U}(\bar{S}) = \frac{TU(S)}{S_m};
\end{aligned}
$$

we obtain the following dimensionless model:

$$-\nabla^2_{(\bar{x},\bar{z})}\bar{p} = \bar{g}(\bar{U})\chi_{\Omega_2(t)} \quad \text{in } \Omega, \tag{9}$$

$$[\bar{p}] = d_0\kappa \quad \text{on } \Gamma, \tag{10}$$

$$[\bar{p}_{\bar{n}}] = 0 \quad \text{on } \Gamma, \tag{11}$$

$$\bar{p} = 0 \quad \text{on } \bar{z} = 1, \tag{12}$$

$$\bar{p}_{\bar{z}} = 0 \quad \text{on } \bar{z} = 0, \tag{13}$$

$$\bar{p}(0,\bar{z}) = \bar{p}(\bar{L}_X,\bar{z}) \quad \forall \bar{z} \in (0,1), \tag{14}$$

$$\bar{S}_{\bar{t}} + \nabla_{(\bar{x},\bar{z})}\cdot(\bar{S}\bar{\mathbf{u}}) - \frac{D_S T}{L_Z^2}\nabla^2_{(\bar{x},\bar{z})}\bar{S} = -\bar{U}(\bar{S})\chi_{\Omega_2(t)} \quad \text{in } \Omega, \tag{15}$$

$$[\bar{S}] = 0 \quad \text{on } \Gamma, \tag{16}$$

$$[\bar{S}_{\bar{n}}] = 0 \quad \text{on } \Gamma, \tag{17}$$

$$\bar{S} = 1 \quad \text{on } \bar{z} = 1, \tag{18}$$

$$\bar{S}_{\bar{z}} = 0 \quad \text{on } \bar{z} = 0, \tag{19}$$

$$\bar{S}(0,\bar{z}) = \bar{S}(\bar{L}_X,\bar{z}) \quad \forall \bar{z} \in (0,1). \tag{20}$$

The key parameters of the dimensionless model are d_0 the *amalgamated* surface tension coefficient (with dimension of length) (see p. 272 in [25]), G, the growth number of the biofilm and ν, which are defined by

$$d_0 = \frac{\lambda\gamma\nu}{D_S G}, \tag{21}$$

$$G = \frac{L_Z^2 U_{Sm}}{D_S S_m}, \tag{22}$$

$$\nu = \frac{TU_{Sm}}{S_m}. \tag{23}$$

The growth number G is a dimensionless quantity representing, in one parameter, the factors that many researchers have found to affect the biofilm structure: the vertical length, since this is the direction in which the substrate diffuses, the concentration of soluble nutrient in the bulk, S_m; its diffusion coefficient D_S, and the maximum substrate consumption rate, U_{Sm}. High G makes the biofilm structure more heterogeneous. At low G, the resulting structure is more compact and homogeneous (see [3]). In the numerical section, we refer these two scenarios as substrate transport limited regime (high

G or low d_0) and growth limited regime (low G or high d_0) respectively. Another important parameter, involved in the definition of the dimensionless pressure $\bar{p}$ and of d_0, is ν which measures the ratio between the time scale of biofilm growth, T, and the substrate consumption time, S_m/U_{Sm}, near the top of the biofilm.

4. Numerical methods

In what follows, we describe the numerical methods required to solve our model, namely, Eqs. (9)–(20). We note that the unknowns of our model are: $\bar{p}$, $\bar{S}$ and Γ. The equations for $\bar{p}$ and $\bar{S}$ are the biofilm balance (9), together with their boundary conditions, and the substrate balance (15), together with their boundary conditions, respectively.

4.1. Numerical method for the interface evolution

The method we have used to compute the interface evolution is the level set method, which was introduced by S. Osher and J.A. Sethian [26]. The central idea of the level set method is to define a smooth (at least Lipschitz continuous) function $\phi(x, z, t)$, called the level set function, that represents the unknown interface as the set where $\phi(x, z, t) = 0$. Therefore, the interface is to be captured for all later times by locating the set $\Gamma(t)$ for which ϕ vanishes. The motion of the interface is analyzed by convecting the values of ϕ (level sets of ϕ) with the velocity field $\mathbf{u}$. This elementary equation is as follows:

$$\phi_t + \mathbf{u} \cdot \nabla\phi = 0.$$

The dimensionless form of the previous equation is

$$\phi_{\bar{t}} + \bar{\mathbf{u}} \cdot \nabla_{(\bar{x},\bar{z})}\phi = 0. \tag{24}$$

We add an initial condition, which implicitly represents the initial interface (i.e., the zero level set of the initial level set function corresponds to the initial interface).

The numerical method we have used to solve Eq. (24) is a combination of the second-order TVD RK approximation [28] to update ϕ from time t_n to t_{n+1} with the second-order ENO approximation to $\nabla_{(\bar{x},\bar{z})}\phi$, as devised in [29]. See also the book by S. Osher and R. Fedkiw (see pp. 31–33 in [27]). Of course, in order to guarantee the stability of the numerical method, we have taken the usual CFL time-step restriction:

$$\Delta t < \frac{h}{\max|\bar{\mathbf{u}}|}.$$

Implicit in the level set method is the fact that $\phi(x, z, t)$ corresponds to the signed normal distance from the point (x, z) to the interface $\Gamma(t)$. This is considering the definition of the level set function, which takes a negative value in the biofilm compartment, positive in the liquid region, and zero at the interface. Although Eq. (24) transports the interface at the right velocity $\bar{\mathbf{u}}$, it is generally not valid to say that ϕ coincides with the signed normal distance to the interface. To overcome this difficulty, we have used the reinitialization process, which consists in solving the following Hamilton–Jacobi equation:

$$\begin{cases} \psi_\tau + \mathrm{Sg}(\phi)(|\nabla\psi| - 1) = 0, \\ \psi(x, z, 0) = \phi(x, z, t), \end{cases} \tag{25}$$

where $\phi(x, z, t)$ corresponds to the level set function calculated by solving Eq. (24) at one temporal iteration, and $\mathrm{Sg}(\phi)$ is the one dimensional sign function composed of ϕ. The idea is to solve (25) performing enough temporal iterations ($\tau \to \infty$) in order to numerically obtain that $|\nabla\psi| \approx 1$. The new function ψ calculated in this way satisfies the property of having the same level sets as ϕ and, in particular, preserves the right position of the interface. Moreover, it is the signed normal distance to the interface.

The reinitialization can be quite complicated, expensive, and have subtle by-products. In [30], the reinitialization is achieved by solving Eq. (25) to its steady state, by choosing a certain approximation of $\mathrm{Sg}(\phi)$. This approach works well when the level set function ϕ is initially not far away from a distance function, but may become too slow when ϕ is flat near the interface, or even worse, it may move the interface across the grid points when the interface becomes steep. Thus we have used a variant of the method introduced by Sussman et al. [30], which has been proposed by Peng et al. [31]. In this variant, the sign function $\mathrm{Sg}(\phi)$ is approximated in a different way to ensure that the interface does not move across the grid points, if it moves at all. Another practical question addressed by [31] is the fact that one does not need to reinitialize the level set function every time step. Indeed, reinitialization every time step is necessary when the interface undergoes a rapid change and ϕ deviates dramatically away from the signed distance function. Otherwise this is excessive. In our simulations, as we model biofilm formation, whose structure has a time scale $>10^5$ sec. (approx. a day) (see p. 57 in [2]), it is clear that the biofilm/liquid interface does not undergo a rapid change and thus ϕ does not deviate too much from the signed distance function. Moreover, from the discussion in [21], the reinitialization plays a role of geometric regularization and stabilizing high frequency components of the solution. Thus if one reinitializes too much, starting from an almost flat interface, this behavior will remain as the time evolves, and therefore the simulation will not necessarily show the real biofilm growth, which depending on the parameters, it has been shown that irregular structures may occur, as discussed in previous sections. In fact, for very unstable problems, the different reinitialization process will affect the computational results, including the

location of the interface [21]. Thus, in our simulations we have obtained the best results when we have carried out the reinitialization every 15 time steps, and by checking convergence of this procedure in a narrow tube of different width for each simulation.

Remark 4.1. It is worth noting that the main difference between our approach and that of Dockery and Klapper [8] is the fact that our pressure equation is written in the entire domain Ω and, indeed, it experiments a jump across the interface Γ. Therefore, it is natural to impose transmission conditions on the interface Γ ((10) and (11)) in order to determine its dynamics. Moreover, we do not assume that the liquid is at rest. It has been shown that a potentially important phenomenon in the analysis of the overall biofilm system includes the effects of fluid motion and advective substrate transport in and out of the biofilm [1] (see p. 104 and the references cited therein [2]). In our case, even if we have taken into account the flow field induced by the motion of the biofilm/liquid interface (and not a flow field induced by the bulk-liquid itself), this induces an advective substrate transport whose contribution could be significant. In contrast, the pressure equation used in [8] is written only for the biofilm compartment, with a Dirichlet boundary condition ($\bar{p} = 0$) at the interface Γ; moreover these authors do not consider the influence of the fluid motion (neither induced by the bulk-liquid nor by the motion of the biofilm/liquid interface) nor the advective substrate transport. On the other hand, since shape and position of the interface are unknowns in our model, it is reasonable to set conditions that take into account the motion of the interface. Indeed, we have modeled such dynamics by using a system of equations, which is based on the Hele-Shaw flow. Finally, from a numerical point of view and in reference to [8], the pressure equation is solved in the biofilm compartment and the biofilm/liquid front line is directly moved by advection of the level set function as a passive scalar by using the velocity field inside the biofilm and linearly extending the pressure across the interface. This is done in order to create an advection velocity field in the liquid region near the interface, which is smoothed to zero away from the interface. By contrast, our method follows natural conditions since the pressure is computed in the whole domain Ω, describing appropriate transmission conditions to capture the motion of the interface so that we do not need to extend the pressure to reproduce the interfacial motion.

4.2. Numerical method for solving the substrate equation

In the sequel, by simplicity, we shall omit the "bar" in the notation for the dimensionless variables. For instance, we shall write p instead of $\bar{p}$, S instead of $\bar{S}$ and so on.

In order to solve (15), together with the boundary conditions (18)–(20), we have used a fractional step method (see pp. 237–239 in [32]). Thus, we split (15) into three equations:

$$S_t - \frac{D_S T}{L_Z^2}\nabla^2 S = 0 \quad \text{in } \Omega, \tag{26}$$

$$S_t + \nabla \cdot (S\mathbf{u}) = 0 \quad \text{in } \Omega, \tag{27}$$

$$S_t = -U(S)\chi_{\Omega_2(t)} \quad \text{in } \Omega. \tag{28}$$

The numerical solution of (15) is then achieved in three steps. In the first step, we solve Eq. (26) for initial data S^n, in the second step we solve Eq. (27) whose initial data is the numerical solution obtained in the first step, and finally, in the third step we solve Eq. (28) whose initial data is the numerical solution obtained in the second step. Next, we will explain each one of the steps.

Step 1. In this step we solve (26), which is a standard parabolic equation. Thus, at each time step, we solve Eq. (26) together with the boundary conditions (18)–(20), by means of the semi-implicit Crank–Nicolson scheme (see pp. 195–196 in [32]). At every time step, we solve the resulting linear system by means of the GMRES algorithm, starting from an initial guess given by the forward Euler method for Eq. (26), which converges in few iterations (see pp. 96–99 in [32]).

Step 2. In this step we have to solve (27) with initial data given by the numerical solution of Step 1. Eq. (27) is an advection equation, whose numerical solution has been approximated by the same method as for level-set Eq. (24).

Step 3. In this step we have to solve (28) with initial data given by the numerical solution of Step 2. Eq. (28) is a reaction equation, whose numerical solution was computed by using an exponential time differencing method (see pp. 240–242 in [32]).

4.3. Numerical method for solving the pressure equation

In this subsection we explain how the biofilm balance equation (9) has been solved:

$$\nabla^2 p = -\delta_g \nu \frac{\mu_m S_m}{U_{Sm}}\left[(1+\mu)\frac{S}{S+K} - \mu\right]\chi_{\Omega_2(t)} \quad \text{in } \Omega. \tag{29}$$

Here above, $K = K_S/S_m$ is the dimensionless Monod saturation constant.

In order to solve Eq. (29) together with the transmission/boundary conditions (10)–(11), and (12)–(14), respectively, a suitable numerical method is needed. This is because the pressure is discontinuous at the interface, and therefore it has to

be accurately approximated across it, which is a fact that guarantees a good approximation, as well as for the velocity $\mathbf{u}$, which is given (under dimensionless form) by $\mathbf{u} = -\nabla p$.

In practice, the approximation of the derivatives of p is the same as for S, except that at those grid points which are near of the interface, the finite difference formula must be adjusted. This is done by adding a corrector term on the right-hand side of the numerical equation, so as to impose the transmission conditions that satisfy p at the interface, in such a way that a high accuracy is achieved in the numerical reconstruction of the solution. This is the main principle of the immersed interface method (IIM). This method was first introduced to deal with partial differential equations whose solution or coefficients, as well as its gradients in the normal direction, may have a jump of discontinuity at the interface. The interested reader is referred to the book by Li and Ito [25] for more details.

Next, a short description of the IIM is given. The numerical approximation for p^{n+1} is based upon the classical centered five-point finite difference scheme. Eq. (29) is solved by means of the centered five-point finite difference scheme:

$$\nabla_h^2 p_{i,j}^{n+1} = -\delta_g \nu \frac{\mu_m S_m}{U_{Sm}} \left[(1+\mu) \frac{S_{i,j}^n}{S_{i,j}^n + K} - \mu \right] \chi_{\Omega_2^n} + C_{i,j}^n, \tag{30}$$

$\forall i = 0, \ldots, N_X, \forall j = 0, \ldots, N_Z$. Here above, $\nabla_h^2 p^{n+1}$ is the discrete Laplace operator, computed by using the centered five-point finite difference scheme, $\chi_{\Omega_2^n}$ is the characteristic function of Ω_2^n (the biofilm compartment at time t_n), $S_{i,j}^n$ is the numerical solution to (15), and $C_{i,j}^n$ is a corrector term which acts only on the *irregular grid points* (i, j). A grid point (i, j) is called an *irregular grid point* in reference to the standard 5-point finite difference stencil centered at (i, j) if the five grid points are not on the same side of the interface. By contrast, the grid points whose standard five-point stencil centered around it is located only on one side of the interface are called *regular grid points*.

Thus,

$$C_{i,j}^n = \begin{cases} 0 & \text{if } (i,j) \text{ is a regular grid point,} \\ \neq 0 & \text{if } (i,j) \text{ is an irregular grid point.} \end{cases}$$

Since the irregular grid points are adjacent to the interfacial curve and form a lower-dimensional set, it turns out to be sufficient to require an $O(h)$ truncation error at these points. Roughly speaking, the idea behind obtaining the corrector terms is as follows: let (i, j) be an irregular grid point, and let us denote by $(i + i_k, j + j_k)$ the grid points of the standard five-point stencil centered at (i, j) (each i_k, j_k takes values in the set $\{-1, 0, 1\}$). Let us expand $p^{n+1}(x_{i+i_k}, z_{j+j_k})$ around a point (x_i^*, z_j^*) at the interface, close to (x_i, z_j) (for example the projection of (x_i, z_j) on the interface). Then, by using the interface relations (10)–(11), and imposing that the truncation error at (x_i, z_j) is $O(h)$, the desired corrector term $C_{i,j}^n$ is obtained. For a complete review of the IIM, we recommend to the interested reader the Refs. [7,25].

Note that the matrix of the resulting system for (30) does not change with the application of the IIM, because we just have to change the right-hand side, and moreover it does not change with the time iterations. Thus, we compute the solution by means of the *LU* factorization of the matrix system, which is only computed once before of the time iterations. Once p is calculated the velocity of the medium, has to be computed, which is given by $\mathbf{u} = -\nabla p$. Again, this is computed by using classical finite difference formulae at regular grid points, and by using a corrector term as devised by the IIM, at irregular grid points [7,25].

4.4. Summary of the algorithm

We can summarize our algorithm as follows:

1. $n \leftarrow 0$. Initialize the initial interface, i.e., initialize the level-set function $\phi(x, z, t = 0)$. Moreover, at time zero, substrate is at its maximum concentration and uniformly distributed in the space $S(x, z, t = 0) = 1$ for all $(x, z) \in \Omega$.
2. Solve Eq. (29) with transmission and boundary conditions (10)–(11) and (12)–(14), respectively, and compute $\mathbf{u} = -\nabla p$ based on the IIM, at time $t_n = n\Delta t$, as explained in Section 4.3. The time-step Δt is chosen in such a way that the level-set Eq. (24) be numerically stable, as explained in Section 4.1.
3. Solve Eq. (24) at time $t_n = n\Delta t$, with $\mathbf{u} = -\nabla p$, and reinitialize ϕ by solving Eq. (25), as explained in Section 4.1. The zero level-set of ϕ gives us the new position of the interface.
4. Solve Eq. (15) coupled with the boundary conditions (18)–(20) at time $t_n = n\Delta t$, as explained in Section 4.2.
5. Change $n \leftarrow n + 1$. Repeat steps (2)–(5) to let the system evolve.

5. Numerical results and discussion

We have done numerical experiments with the same initial biofilm–liquid interface and different growth numbers (or surface tensions). The crucial parameter which affects the stability in the Hele-Shaw flow is the amalgamated surface tension coefficient d_0, and thus the growth number G (see (21)). The greater the G (or lower the d_0), the more unstable the Hele-Shaw flow [21]. Below some results and analysis are presented. In all the simulations the time is in hours.

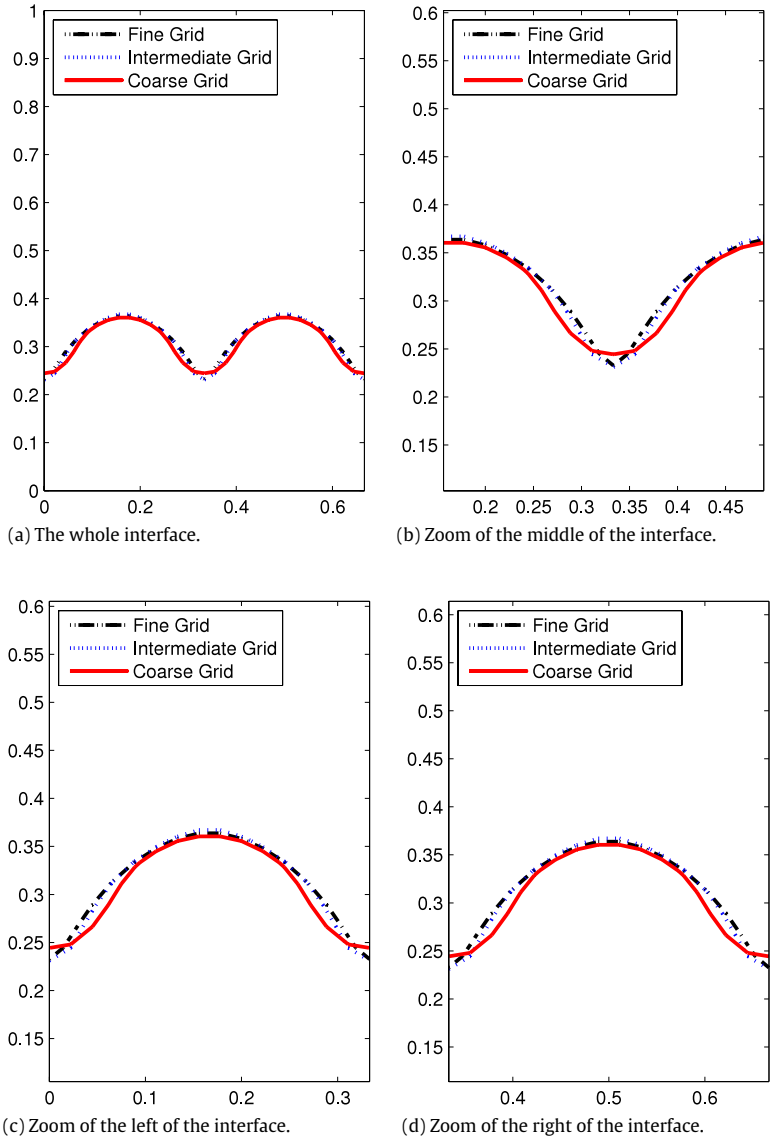

(a) The whole interface. (b) Zoom of the middle of the interface.

(c) Zoom of the left of the interface. (d) Zoom of the right of the interface.

Fig. 1. Grid refinement analysis for the first simulation. Convergence is observed.

5.1. Grid refinement analysis

In this subsection we present a grid refinement analysis of our numerical method. To demonstrate the convergence of our method, we carry out our analysis for three different simulations. The first one consists of an initial condition representing an already formed homogeneous biofilm layer. To do this we take an interface which is a perturbed horizontal straight line, defined implicitly by the level set function:

$$\phi_0(x, z) = (z - L_Z/4) + 0.02\cos(4\pi x/L_X). \tag{31}$$

We start our study with a uniform grid of 30 intervals in the x-direction and 45 in the z-direction, and double it twice to conduct the grid refinement analysis. In the sequel of this section, we refer as the coarse grid that is composed of 30 intervals in the x-direction and 45 in the z-direction (whose grid step size is $h = 1/45 = 0.0222$), as the intermediate grid that is composed of 60 intervals in the x-direction and 90 in the z-direction (whose grid step size is $h = 0.0111$), and by the fine grid that is composed of 120 intervals in the x-direction and 180 in the z-direction (whose grid step size is $h = 0.0056$), respectively.

As discussed in Section 4.1, we have applied the reinitialization procedure [31] every 15 time iterations for the three grids. If we apply the reinitialization too many times for the coarse grid, then we will not allow the biofilm to grow, because the reinitialization plays a role of geometric regularization. Thus, starting from a homogeneous biofilm, the reinitialization

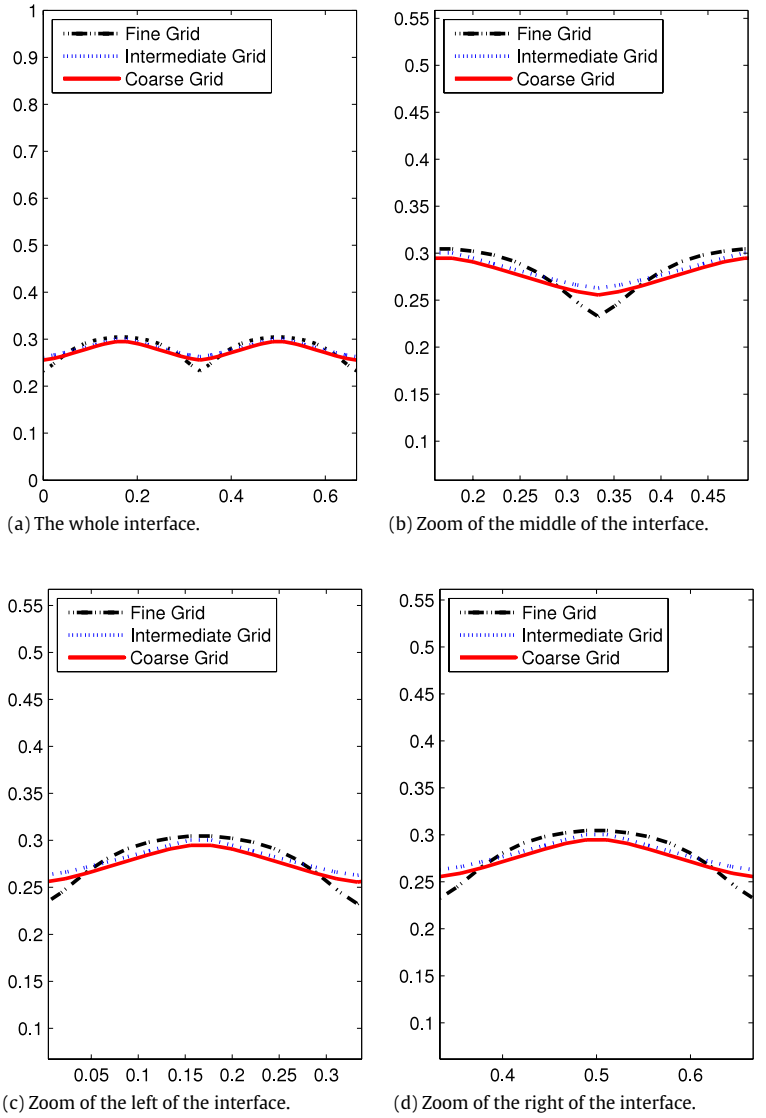

(a) The whole interface.

(b) Zoom of the middle of the interface.

(c) Zoom of the left of the interface.

(d) Zoom of the right of the interface.

Fig. 2. Grid refinement analysis for the second simulation. Convergence is observed.

prevents the development of irregular forms in the biofilm structure, which is observed in real biofilms and also in biofilm model simulations for a transport-limited regime (high metabolic rates, that is, high G) [6]. Moreover, the application of reinitialization every time iteration is required only when the interface undergoes a rapid change and the level-set function deviates too much from the signed distance function [31]. In this sense, we have found that our simulations describe well the biofilm formation when we apply the reinitialization procedure every 15 time iterations for the three grids, and by requiring the stopping criterion that leads to impose the condition

$$|\nabla\phi| = 1 + O(h^2),$$

for the reinitialized level set function ϕ, on the grid points located in a tube about the interface, where h is the grid size.

The actual version of the model code was run on an Intel Core Duo CPU P9600 machine at 2.67 GHz. Typical runs take several hours of computations. For instance, 1440 time iterations take 1468 s, in the finest grid.

We present our first grid refinement analysis for

$$G = 395, \qquad S_m = 4 \cdot 10^{-3}\ \text{kg m}^{-3},$$

for a transport-limited regime (high metabolic rates). The values for the parameters S_m, D_S, K_S and μ_m were obtained from [6]. The parameter U_{Sm} was estimated in order to obey relation (22) for a biofilm of characteristic length $L_Z = 2 \cdot 10^{-3}$ m. The time scale of biofilm growth was taken as $T = 1000$ s [20]. The parameter γ is the surface tension of the water (see

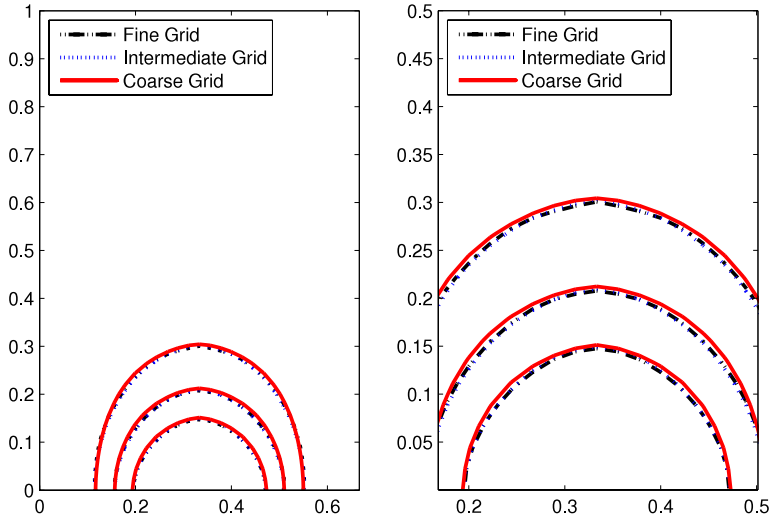

(a) The whole interface. (b) Zoom of the interface.

Fig. 3. Grid refinement analysis for the third simulation. Convergence is observed.

p. 408 in [33]). The parameters ν and d_0 were derived from the values of the other parameters according to (21) and (23), respectively. The parameter μ was estimated in the order of a usual maintenance coefficient [4], λ was estimated in order to take into account that the biofilm behaves as a fluid with large viscosity (λ has to be small as discussed in Section 2) and particularly to obtain d_0 in a reasonable physical range [21] (see (21)). Finally the scaling parameters δ_U and δ_g were estimated in order to reproduce the desired behavior (mushroom-shaped biofilm/liquid interface for high G and low S_m, and more compact and homogeneous biofilm structure for low G and high S_m). The values for the parameters D_S, K_S, μ_m and T are the same through all the simulations, whereas the values for G, S_m, U_{Sm}, d_0, μ, ν, δ_U and δ_g were varied in order to simulate other behaviors (such as biofilm growth-limited regime). See Table 1 for a list of the common parameters. See also Table 2 for a list of the parameters used in the first simulation.

The way to calculate the errors is explained below. We estimate the error on each grid by using the next finer grid as the reference solution, rather than using the same reference solution for both coarser grids. More precisely, we compute the errors at each time t as follows:

$$E_h(t) = \|\phi_h(t) - \phi_{h/2}(t)\|_{L^1(\Gamma_h)}/M_h,$$
$$E_{h/2}(t) = \|\phi_{h/2}(t) - \phi_{h/4}(t)\|_{L^1(\Gamma_{h/2})}/M_{h/2},$$

where M_h (resp. $M_{h/2}$) stands by the number of grid points in $T_h = \{|\phi_h| \leq \alpha_h\}$ (resp. $T_{h/2} = \{|\phi_{h/2}| \leq \alpha_{h/2}\}$), where α_h (resp. $\alpha_{h/2}$) is the tube width T_h (resp. $T_{h/2}$) for the reinitialization procedure corresponding to the coarse (resp. intermediate) grid. Errors E_h and $E_{h/2}$ measure the difference of the computed level-set functions in (averaged) L^1-norm in the tube where we test the convergence of our reinitialization procedure (see [30]), that is, we measure the errors in a vicinity of the interface, because its location and shape are the best indicators of the convergence of our method. In order to determine the order of convergence, we examine the ratio $E_{h/2}/E_h$, which should be at most 0.25 if the method is second-order accurate (see [32, pp. 257–258]). See Table 3 for a list of the numerical parameters α_h used in each simulation.

Fig. 1 qualitatively demonstrates the convergence of our method as we refine the mesh. The figure depicts the zero level set of ϕ (the biofilm/liquid interface) at time $t = 17.6056$. Table 4 depicts quantitatively the grid refinement analysis at three different times, by showing the computed errors as explained before. The results in Table 4 clearly indicate second-order accuracy at three different times.

Our second simulation consists in the same initial condition as for the first simulation (see (31)), but with different parameters. See Table 5 for a list of the parameters used in the second simulation. The results in Table 6 clearly show second-order accuracy at three different times. Fig. 2 qualitatively shows convergence for the second simulation at time $t = 0.1956$.

Our third simulation consists in a semicircular biofilm colony growing towards the substrate source (the top of the domain). The initial condition is given by the level set function:

$$\phi_0(x, z) = \sqrt{(x - L_X/2)^2 + z^2} - 0.11.$$

The parameters for this simulation are given in Table 7. The results in Table 8 clearly show second-order accuracy at three different times. Fig. 3 qualitatively shows convergence for the third simulation at the three different times given in Table 8.

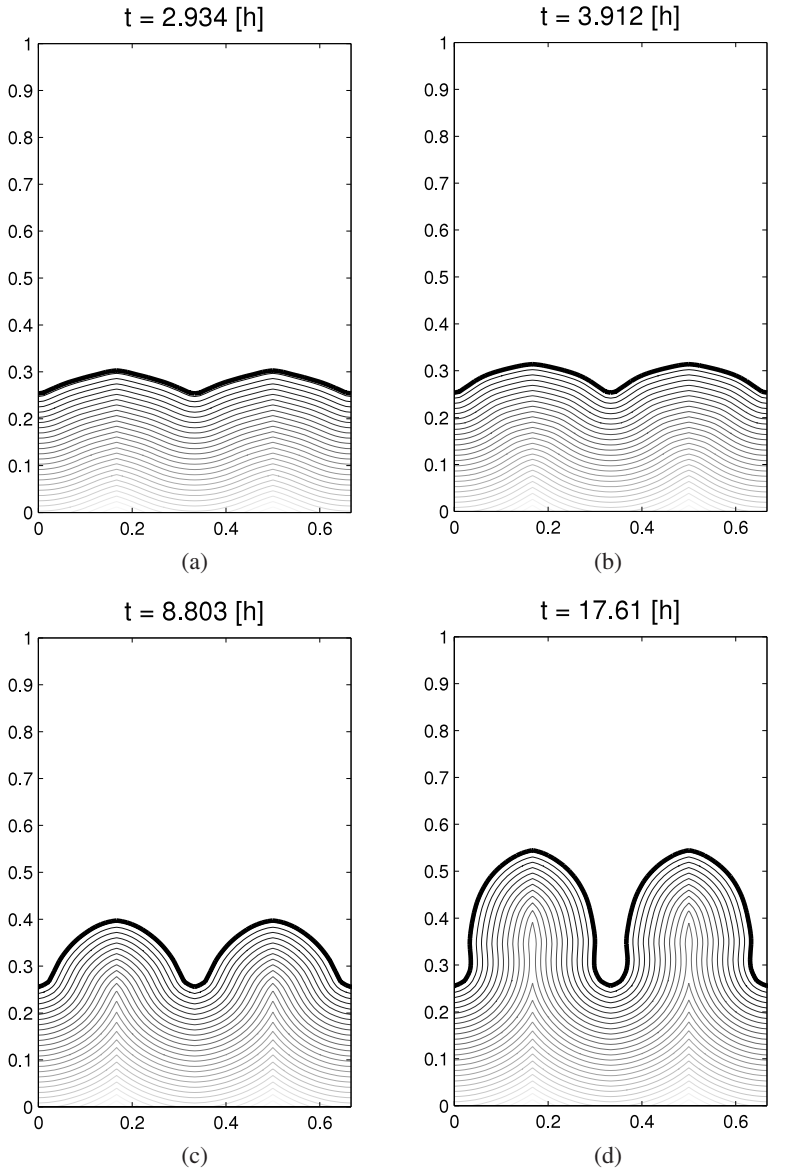

Fig. 4. Four different snapshots of a mushroom-shaped biofilm, simulated with the intermediate grid (first simulation).

Table 1
Common parameters to all simulations.

Parameter	Symbol	Value	Units
Time scale of biofilm growth	T	1000	s
Monod half-saturation constant	K_S	$3.5 \cdot 10^{-4}$	$\mathrm{kg\,m^{-3}}$
Diffusion coefficient	D_S	$2.3 \cdot 10^{-9}$	$\mathrm{m^2\,s^{-1}}$
Surface tension coefficient in water	γ	$72.8 \cdot 10^{-3}$	$\mathrm{kg\,s^{-2}}$
Maximum specific growth rate	μ_m	$1.5 \cdot 10^{-5}$	$\mathrm{s^{-1}}$

5.2. Further experiments and analysis

Below we compare our results with those obtained in the literature. We compare the first two simulations shown in the grid refinement analysis: the first one for $G = 395$ and $S_m = 4 \cdot 10^{-3}$ kg m^{-3}, for a transport-limited regime, and the second one for $G = 16$ and $S_m = 1 \cdot 10^{-1}$ kg m^{-3}, for a growth-limited regime, starting from the same initial condition (31).

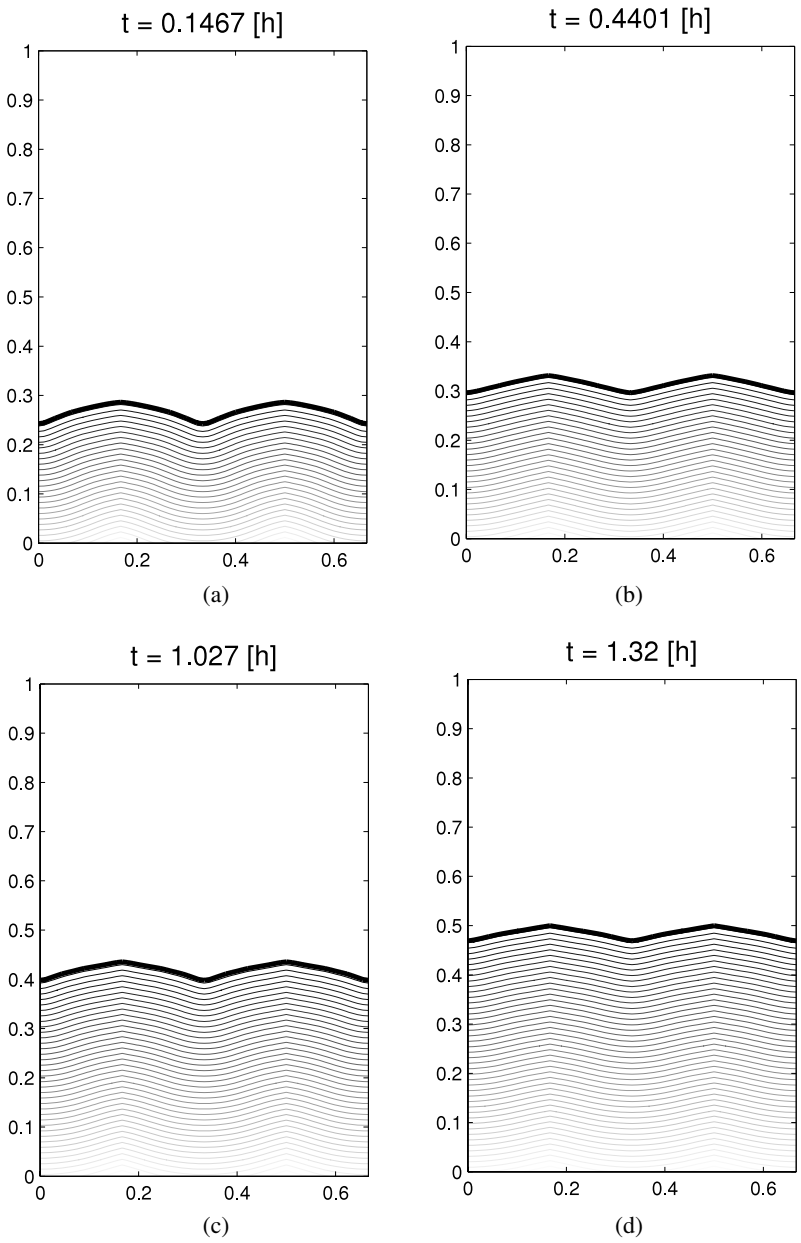

Fig. 5. Four different snapshots of a compact-shaped biofilm, simulated with the intermediate grid (second simulation).

Table 2
Parameters used in the first simulation.

Parameter	Symbol	Value	Units
System dimensions			
Length	L_X	$1.333 \cdot 10^{-3}$	m
Height	L_Z	$2 \cdot 10^{-3}$	m
Substrate concentration in the bulk liquid	S_m	$4 \cdot 10^{-3}$	kg m^{-3}
Maximum substrate consumption rate	U_{Sm}	$9.088 \cdot 10^{-4}$	kg m^{-3} s^{-1}
Ratio between biofilm growth and substrate consumption	ν	$4.4014 \cdot 10^{-3}$	Dimensionless
Proportionality coefficient in pressure equation	λ	$4.4014 \cdot 10^{-11}$	kg^{-1} m^3 s
Maintenance coefficient	μ	$1.3204 \cdot 10^{-4}$	Dimensionless
Amalgamated surface tension	d_0	$8.0106 \cdot 10^{-4}$	m
Scaling parameter for U	δ_U	$8 \cdot 10^{-3}$	Dimensionless
Scaling Parameter for g	δ_g	$6.6021 \cdot 10^{-4}$	Dimensionless

Table 3
Tube width used in each simulation.

Grid	First	Second	Third
Coarse	1/350	1/40	1/230
Intermediate	1/340	1/400	1/305
Fine	1/1250	1/250	1/720

Table 4
Grid refinement analysis for the first simulation.

Time	E_h	$E_{h/2}$	$E_{h/2}/E_h$
5.8685	$4.1248 \cdot 10^{-6}$	$1.7253 \cdot 10^{-7}$	0.0418
11.7371	$4.6715 \cdot 10^{-6}$	$4.9488 \cdot 10^{-7}$	0.1059
17.6056	$4.3121 \cdot 10^{-6}$	$3.1629 \cdot 10^{-7}$	0.0733

Table 5
Parameters used in the second simulation.

Parameter	Symbol	Value	Units
System dimensions			
Length	L_X	$1.1926 \cdot 10^{-4}$	m
Height	L_Z	$1.7889 \cdot 10^{-4}$	m
Substrate concentration in the bulk liquid	S_m	$1 \cdot 10^{-1}$	kg m^{-3}
Maximum substrate consumption rate	U_{Sm}	$1.136 \cdot 10^{-1}$	kg m^{-3} s^{-1}
Ratio between biofilm growth and substrate consumption	ν	$8.8028 \cdot 10^{-4}$	Dimensionless
Amalgamated surface tension	d_0	$2.00 \cdot 10^{-2}$	m
Proportionality coefficient in pressure equation	λ	$8.8028 \cdot 10^{-12}$	kg^{-1} m^3 s
Maintenance coefficient	μ	$2.6408 \cdot 10^{-5}$	Dimensionless
Scaling parameter for U	δ_U	$7.0423 \cdot 10^{-2}$	Dimensionless
Scaling parameter for g	δ_g	$7.0423 \cdot 10^{-3}$	Dimensionless

Table 6
Grid refinement analysis for the second simulation.

Time	E_h	$E_{h/2}$	$E_{h/2}/E_h$
0.1467	$2.5060 \cdot 10^{-6}$	$5.4183 \cdot 10^{-7}$	0.2162
0.1956	$5.0392 \cdot 10^{-6}$	$8.7318 \cdot 10^{-7}$	0.1733
0.2445	$7.7270 \cdot 10^{-6}$	$1.8515 \cdot 10^{-6}$	0.2396

Table 7
Parameters used in the third simulation.

Parameter	Symbol	Value	Units
System dimensions			
Length	L_X	$1.3333 \cdot 10^{-3}$	m
Height	L_Z	$2 \cdot 10^{-3}$	m
Substrate concentration in the bulk liquid	S_m	$4 \cdot 10^{-3}$	kg m^{-3}
Maximum substrate consumption rate	U_{Sm}	$9.088 \cdot 10^{-4}$	kg m^{-3} s^{-1}
Ratio between biofilm growth and substrate consumption	ν	$4.4014 \cdot 10^{-3}$	Dimensionless
Amalgamated surface tension	d_0	$8.0106 \cdot 10^{-4}$	m
Proportionality coefficient in pressure equation	λ	$4.4014 \cdot 10^{-11}$	kg^{-1} m^3 s
Maintenance coefficient	μ	$1.3204 \cdot 10^{-4}$	Dimensionless
Scaling parameter for U	δ_U	$3.1 \cdot 10^{-2}$	Dimensionless
Scaling parameter for g	δ_g	$1.3644 \cdot 10^{-2}$	Dimensionless

Table 8
Grid refinement analysis for the third simulation.

Time	E_h	$E_{h/2}$	$E_{h/2}/E_h$
0.4450	$1.9491 \cdot 10^{-6}$	$1.0460 \cdot 10^{-7}$	0.0537
0.8900	$1.6364 \cdot 10^{-6}$	$1.6036 \cdot 10^{-7}$	0.0980
1.3351	$1.7299 \cdot 10^{-6}$	$2.4036 \cdot 10^{-7}$	0.1389

The evolution of a biofilm (in hours) is presented in Figs. 4 and 5. In these figures, we have plotted the negative level sets of the level function ϕ (with a variation of $h = 0.0111$ between lines), i.e., those level sets corresponding to the biofilm compartment. The thicker line represents the zero level set of ϕ, and it corresponds to the biofilm/liquid interface.

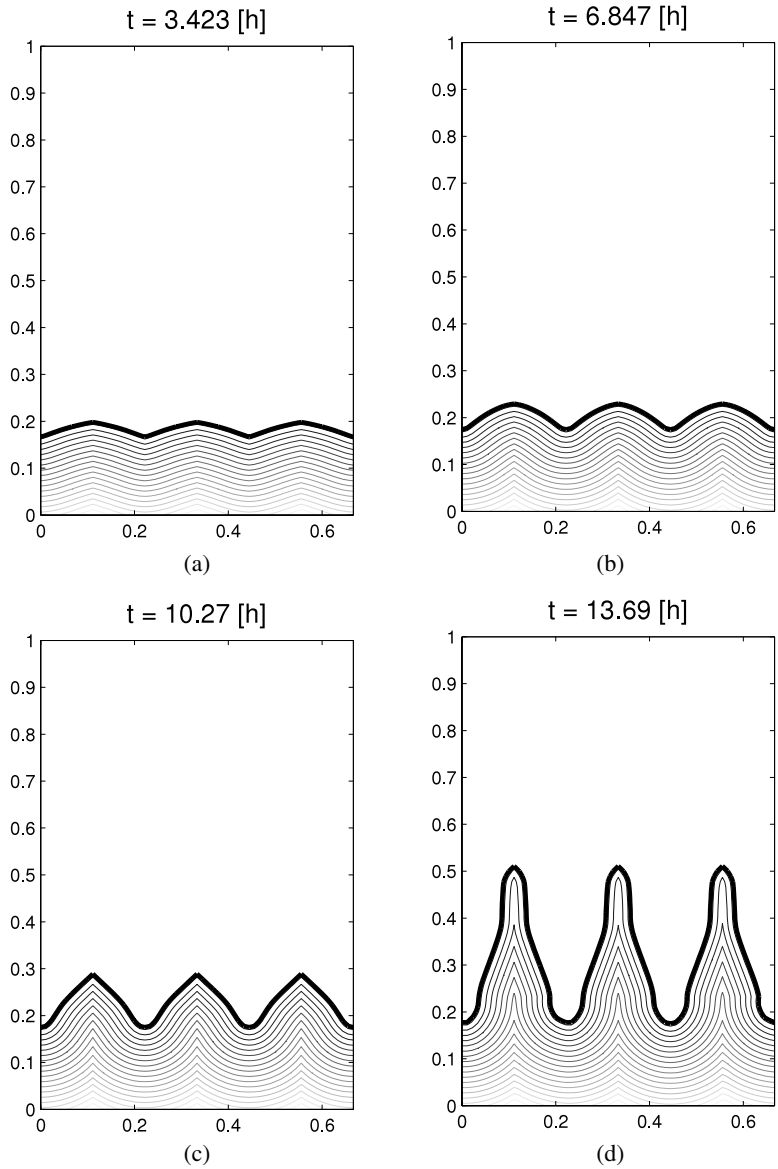

Fig. 6. Four different snapshots of a finger-shaped biofilm, simulated with the intermediate grid (fourth simulation).

At the beginning, when there is sufficient substrate in the environment (i.e., there is no important nutrient limitation), the biofilm grows in all directions (see Fig. 4(a)–(b), and Fig. 5(a)–(b)). As the biofilm gets thicker, two situations can occur. If there is still no substrate limitation (i.e., low G) the biofilm grows forming a relatively compact or smooth structure (see Fig. 5(c)–(d)). The other possible scenario is when the nutrient is depleted in the biofilm depth. In this case, there is almost no flux of substrate to the cells situated in the "valleys". Since only microbes in the top regions are active, dividing and creating new biomass, the biofilm grows forming "finger" or "mushroom" like structures towards the liquid bulk (see Fig. 4(c)–(d)). In general, for homogeneously distributed biomass on the carrier (Fig. 5), the preferential growth direction is perpendicular to the carrier surface. This is consistent with the following fact mentioned in Section 2: the smaller the surface tension d_0 is (the greater the growth number G) the more unstable is the biofilm interface (for a more detailed discussion, see pp. 277–278 in [25,21]).

We can observe the formation of finger-like structures after longer periods of time (see Fig. 4(c)–(d)), which is a common pattern observed in biofilm growth (see Refs. [2–6,8]). In the second simulation (Fig. 5), starting from the same initial interface, but using different values for the parameters than those used in the first simulation, it can be observed that the biofilm arrives to the top of the computational domain (where the source of substrate is located) faster than in the previous simulation. This is because of the growth-limited regime (low G), in whose case there is not an important limitation of substrate. The behavior shown in the two simulations, carried out in this subsection, shows that our model can follow more

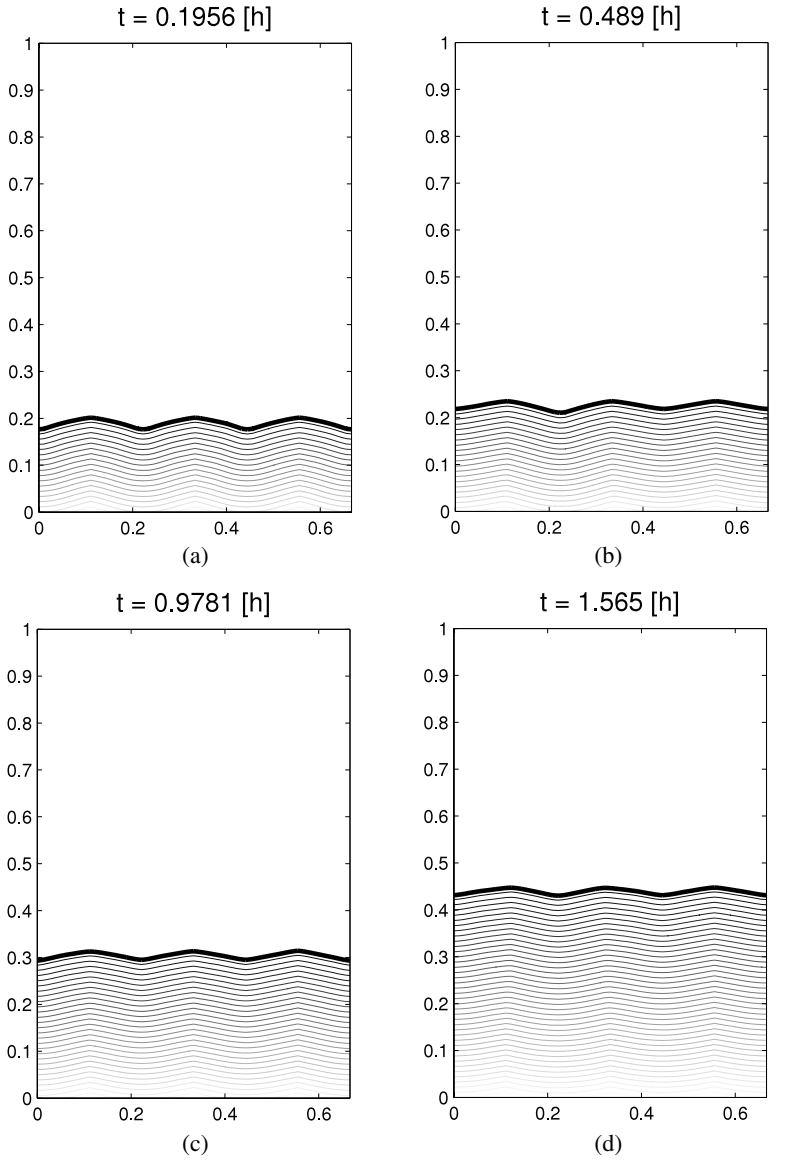

Fig. 7. Four different snapshots of a compact-shaped biofilm, simulated with the intermediate grid (fifth simulation).

smooth development of biofilms structures in the shorter time periods as depicted in Fig. 5 in the second simulation, whereas in longer time periods more pronounced "finger" like structures as depicted in Fig. 4(d). Since this is a numerical solution in which parameters may be adjusted to the specific biofilm that needs to be simulated, it clearly shows that the model proposed in this paper has the potential to simulate a range of behaviors that have been observed in biofilm models and their practical behavior.

The same analysis done before for simulations 1 and 2 also holds true for simulations 4 and 5, which are shown in Figs. 6 and 7 respectively. Finally, to conclude this section, Fig. 8 depicts a semicircular biofilm colony that grows towards the top of the domain (where the source of substrate is located). We see in Fig. 8 that the colony grows forming a finger-like structure.

6. Conclusions

1. A 2-D mathematical model was elaborated for biofilm evolution including biomass growth and decay, diffusive and convective transport, and transformation of substrates and flow around the biofilm structure. This model is different from existing models, since it simulates a biofilm–liquid interface by means of convective biomass transport, instead of spreading biomass concentration under the influence of substrate transport, as was done by [3–6]. On the other hand, the only model that is similar to ours [8] does not include several effects: convective transport of substrate, flow field induced by the motion of the biofilm/liquid interface, and a set of equations describing the evolution of the interface.

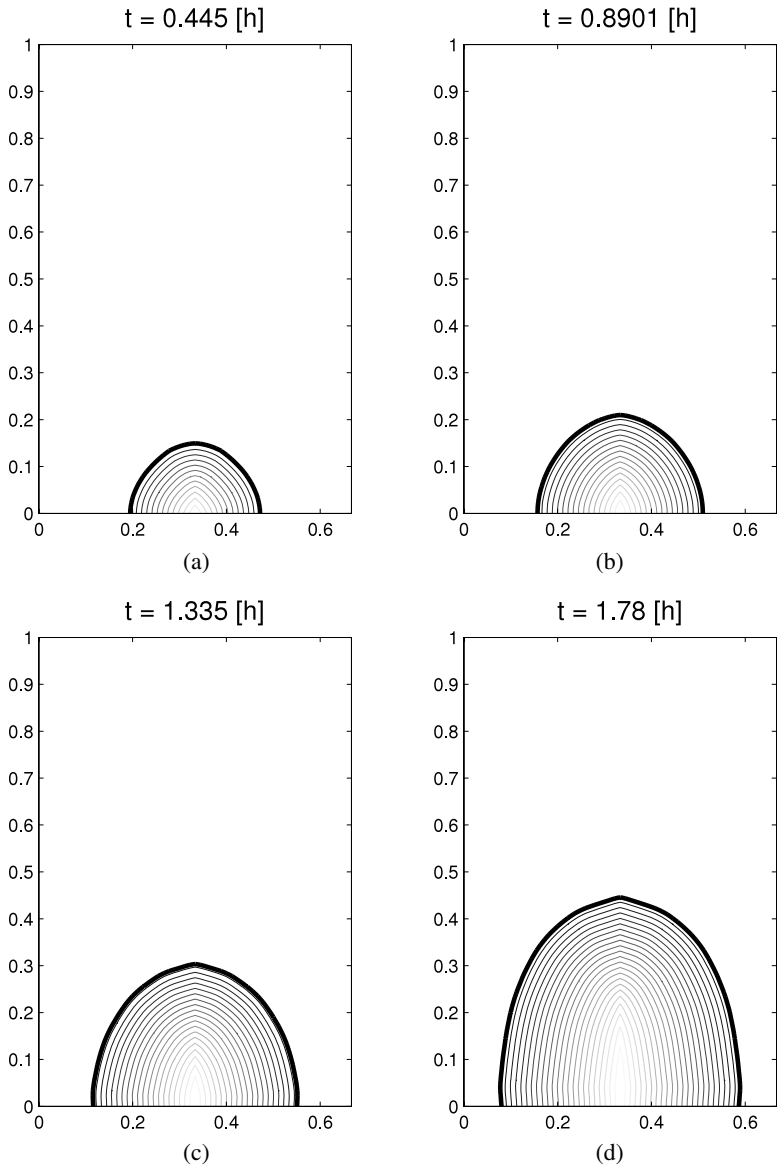

Fig. 8. Four different snapshots of a semicircular biofilm, simulated with the intermediate grid (third simulation).

Indeed, the conditions describing the motion of the interface are a key issue in our model that have been extensively used for describing a wide and growing class of free interface problems (see Chapter 11 in the book [25] and the references cited therein).

2. The evaluation of this model requires the use of sophisticated numerical techniques – the Immersed Interface Method (IIM) coupled to the Level-Set Method – which have been applied for the very first time to the Hele-Shaw flow to solve the increasingly important phenomenon of biofilm growth. The novel approach to biofilm modeling followed in the paper is, as far as we know, for the first time applied in the field of biology, and hence introduces biologists to a method that is likely to find applications.
3. Using this model, we have performed numerical simulations that predict the formation of biofilms in a range of different processes. The use of our model sheds light on the biological process of biofilm formation, since it simulates central issues for biofilm growth: the eventual *pattern formation of heterogeneous structures, such as finger-like structures*. Hence, we have considered the results obtained by [3–6], whose predictions show that structures with high degrees of surface irregularity develop in biofilm growth regimes limited by the rate of substrate transport (internal, as well as external). Biofilms grow in these conditions as "finger-like" or filamentous structures. As the nutrient availability increases, there is a gradual shift towards more compact and smooth biofilms. This is consistent with the fact that the smaller the surface tension d_0 (i.e., the higher the growth number G) is, the more unstable the biofilm interface becomes (see [21] and pp. 277–278 in [25]).

4. The most relevant characteristic of this novel and more rigorous approach, based on existing mathematical analysis, is that it can simulate and follow the behavior of a range of previously described biofilm models that simulate practical biofilm behavior. Detailed comparisons with experimental data should be the result of future research.
5. The model could consider two or more substrates interacting with each other. This amounts to introducing new equations to the model, taking into account transport and interaction of the various substrates.
6. The model could also consider biofilm systems with multiple species [11].
7. In addition, we could consider the flow field induced by the bulk-liquid itself. In this case, the liquid would have its own motion, which should be coupled to the biofilm motion by means of appropriate conditions on the interface.

Acknowledgments

This work was partially supported by Millennium Scientific Initiative under grant number ICM P05-001-F. The work of first author was also partially supported by Chilean Government Fondecyt-Conicyt Program under grant number 11080222 and by Universidad del Bío-Bío (grant DIUBB 121909 GI/C). Third author was also partially supported by Fondecyt grant number 1130317.

References

[1] R. Dillon, L. Fauci, A. Fogelson, D. Gaver, Modeling biofilm processes using the immersed boundary method, J. Comput. Phys. 129 (1) (1996) 57–73.
[2] O. Wanner, H.J. Eberl, E. Morgenroth, D.R. Noguera, C. Picioreanu, B.E. Rittmann, M.C. van Loosdrecht, Mathematical Modeling of Biofilms, IWA Publishing, Alliance House, 2006.
[3] C. Picioreanu, M.C.M. van Loosdrecht, J.J. Heijnen, A new combined differential-discrete cellular automaton approach for biofilm modeling: application for growth in gel beads, Biotechnol. Bioeng. 57 (6) (1998) 718–731.
[4] C. Picioreanu, M.C.M. van Loosdrecht, J.J. Heijnen, Mathematical modeling of biofilm structure with a hybrid differential-discrete cellular automaton approach, Biotechnol. Bioeng. 58 (1) (1998) 101–116.
[5] C. Picioreanu, M.C.M. van Loosdrecht, J.J. Heijnen, A theoretical study on the effect of surface roughness on mass transport and transformation in biofilms, Biotechnol. Bioeng. 68 (4) (2000) 355–369.
[6] C. Picioreanu, M.C.M. van Loosdrecht, J.J. Heijnen, Effect of diffusive and convective substrate transport on biofilm structure formation: a two-dimensional modeling study, Biotechnol. Bioeng. 69 (5) (2000) 504–515.
[7] R.J. LeVeque, Z.L. Li, The immersed interface method for elliptic equations with discontinuous coefficients and singular sources, SIAM J. Numer. Anal. 31 (4) (1994) 1019–1044.
[8] J. Dockery, I. Klapper, Finger formation in biofilm layers, SIAM J. Appl. Math. 62 (3) (2001) 853–869 (electronic).
[9] H.J. Eberl, L. Demaret, A finite difference scheme for a degenerated diffusion equation arising in microbial ecology, in: Proceedings of the Sixth Mississippi State—UBA Conference on Differential Equations and Computational Simulations, in: Electron. J. Differ. Equ. Conf., vol. 15, Southwest Texas State Univ., San Marcos, TX, 2007, pp. 77–96.
[10] C.S. Peskin, Numerical analysis of blood flow in the heart, J. Comput. Phys. 25 (3) (1977) 220–252.
[11] E. Alpkvist, I. Klapper, A multidimensional multispecies continuum model for heterogeneous biofilm development, Bull. Math. Biol. 69 (2) (2007) 765–789.
[12] O. Wanner, W. Gujer, A multispecies biofilm model, Biotechnol. Bioeng. 28 (3) (1986) 314–328.
[13] R. Duddu, S. Bordas, D. Chopp, B. Moran, A combined extended finite element and level set method for biofilm growth, Internat. J. Numer. Methods Engrg. 74 (5) (2008) 848–870.
[14] N. Cogan, Two-fluid model of biofilm disinfection, Bull. Math. Biol. 70 (2008) 800–819.
[15] J.P. Ward, J.R. King, A.J. Koerber, J.M. Croft, R.E. Sockett, P. Williams, Early development and quorum sensing in bacterial biofilms, J. Math. Biol. 47 (2003) 23–55.
[16] K. Anguige, J. King, J. Ward, P. Williams, Mathematical modelling of therapies targeted at bacterial quorum sensing, Math. Biosci. 192 (1) (2004) 39–83.
[17] K. Anguige, J. King, J. Ward, Modelling antibiotic- and anti-quorum sensing treatment of a spatially-structured *pseudomonas aeruginosa* population, J. Math. Biol. 51 (2005) 557–594.
[18] K. Anguige, J. King, J. Ward, A multi-phase mathematical model of quorum sensing in a maturing pseudomonas aeruginosa biofilm, Math. Biosci. 203 (2) (2006) 240–276.
[19] T. Zhang, N.C. Cogan, Q. Wang, Phase field models for biofilms, I. Theory and one-dimensional simulations, SIAM J. Appl. Math. (2008).
[20] T. Zhang, N.G. Cogan, Q. Wang, Phase field models for biofilms II. 2-D numerical simulations of biofilm–flow interaction, Commun. Comput. Phys. 4 (1) (2008) 72–101.
[21] T.Y. Hou, Z. Li, S. Osher, H. Zhao, A hybrid method for moving interface problems with application to the Hele–Shaw flow, J. Comput. Phys. 134 (2) (1997) 236–252.
[22] J.K. Hunter, Z. Li, H. Zhao, Reactive autophobic spreading of drops, J. Comput. Phys. 183 (2) (2002) 335–366.
[23] K. Ito, K. Kunisch, Z. Li, Level-set function approach to an inverse interface problem, Inverse Problems 17 (5) (2001) 1225–1242.
[24] Z. Li, H. Zhao, H. Gao, A numerical study of electro-migration voiding by evolving level set functions on a fixed cartesian grid, J. Comput. Phys. 152 (1) (1999) 281–304.
[25] Z. Li, K. Ito, The Immersed Interface Method: Numerical Solutions of PDEs Involving Interfaces and Irregular Domains, in: Frontiers in Applied Mathematics, vol. 33, Society for Industrial and Applied Mathematics (SIAM), Philadelphia, PA, 2006.
[26] S. Osher, J.A. Sethian, Fronts propagating with curvature-dependent speed: algorithms based on Hamilton–Jacobi formulations, J. Comput. Phys. 79 (1) (1988) 12–49.
[27] S. Osher, R. Fedkiw, Level Set Methods and Dynamic Implicit Surfaces, in: Applied Mathematical Sciences, vol. 153, Springer-Verlag, New York, 2003.
[28] C.-W. Shu, S. Osher, Efficient implementation of essentially nonoscillatory shock-capturing schemes, J. Comput. Phys. 77 (2) (1988) 439–471.
[29] Y.C. Chang, T.Y. Hou, B. Merriman, S. Osher, A level-set formulation of Eulerian interface capturing methods for incompressible fluids flow, J. Comput. Phys. 124 (72) (1996) 449–464.
[30] M. Sussman, P. Smereka, S. Osher, A level set approach for computing solutions to incompressible two-phase flow, J. Comput. Phys. 114 (1994) 146–159.
[31] D. Peng, B. Merriman, S. Osher, H. Zhao, M. Kang, A PDE-based fast local level set method, J. Comput. Phys. 155 (1999) 410–438.
[32] R.J. LeVeque, Finite Difference Methods for Ordinary and Partial Differential Equations: Steady-State and Time-Dependent Problems, Society for Industrial and Applied Mathematics (SIAM), Philadelphia, PA, 2007.
[33] G.W. Castellan, Physical Chemistry, third ed., Addison-Wesley publishing company, 1983.